Pergamon

Int. J. Solids Structures Vol. 35, No. 33, pp. 4457–4476, 1998

0020–7683/98 $19.00 + .00

PII: S0020–7683(97)00253–9

NONLINEAR TRANSIENT THERMOELASTIC ANALYSIS OF FUNCTIONALLY GRADED CERAMIC–METAL PLATES

G. N. PRAVEEN and J. N. REDDY†
Computational Mechanics Laboratory, Department of Mechanical Engineering, Texas A&M University, College Station, TX 77843-3123, U.S.A.

(*Received* 26 *February* 1997; *in revised form* 12 *August* 1997)

Abstract—The response of functionally graded ceramic–metal plates is investigated using a plate finite element that accounts for the transverse shear strains, rotary inertia and moderately large rotations in the von Kármán sense. The static and dynamic response of the functionally graded material (fgm) plates are investigated by varying the volume fraction of the ceramic and metallic constituents using a simple power law distribution. Numerical results for the deflection and stresses are presented. The effect of the imposed temperature field on the response of the fgm plate is discussed. It is found that in general, the response of the plates with material properties between those of the ceramic and metal is not intermediate to the responses of the ceramic and metal plates.

1. INTRODUCTION

Composites are materials with microstructures so tailored as to achieve desired response characteristics. In the case of laminated composite plates, tailoring is achieved commonly by varying the ply thickness, ply material and the stacking sequence. A new class of materials known as "functionally graded materials" (FGMs) has emerged, in which the material properties are graded but continuous. By grading properties in a continuous manner, the disadvantages of interfaces in composites can be mitigated. These materials are microscopically heterogeneous and are typically made from isotropic components, such as metals and ceramics. FGMs are primarily used in situations where large temperature gradients are encountered. FGMs have also found applications in the semiconductor industry.

Thin walled members, i.e., plates and shells, used in reactor vessels, turbines and other machine parts are susceptible to failure from buckling, large amplitude deflections, or excessive stresses induced by thermal or combined thermomechanical loading. Investigations dealing with static and dynamic behavior of isotropic and anisotropic thermoelastic plates have been discussed in detail by Tauchert (1986, 1987). In the present paper, attention is focussed on the thermomechanical response of thick plates, with a continuous variation of properties through the thickness. The temperature is assumed to vary only in the thickness direction. Thermal stresses in free plates under different one-dimensional temperature profiles have been investigated by Schneider (1955). Tang (1968) considered the response of free plates with temperature dependent properties. Bending in plates is generally accompanied by a stretching of the mid-surface when the material properties vary with temperature, but, bending–stretching coupling is shown to disappear in free plates when the temperature varies through the thickness only (Tauchert, 1991).

Das and Navaratna (1962) investigated the bending of rectangular plates, with two parallel edges simply supported, and exposed to a temperature distribution that is symmetric about the middle surface. De Leon and Paris (1987) developed boundary integral formulations based on the decomposition of the field equations into a pair of harmonic equations. Results were presented for a simply supported square plate under a temperature distribution which varied linearly through the thickness.

† Author to whom correspondence should be addressed. Fax: 001-409-845-3081.

Thermoelastic analyses including transverse shear effects were performed by Das and Rath (1972) and Bapu Rao (1979). Das and Rath utilized Levy solutions to solve linear equations for thick rectangular plates with two parallel edges simply supported, and subjected to a temperature distribution which is antisymmetric about the mid plane.

Reddy and Hsu (1980) presented analytical closed-form solution for simply supported rectangular cross-ply laminated plates under sinusoidal mechanical loading. In this analysis, the temperature field was assumed to vary linearly through the thickness, consistent with the kinematics of the first order plate theory used. The governing equations solved in this paper were linear due to the assumption of small strains. Reddy and Chao (1981) studied the effects of reduced integration, mesh size, and element interpolation order on the accuracy of a finite element based on the first order shear deformation plate theory. They also developed exact closed form solutions, in the linear case for the bending of cross-ply and antisymmetric angle-ply rectangular plates, that are simply-supported and subjected to sinusoidally distributed mechanical and thermal loads. Khdeir and Reddy (1991) presented exact analytical solutions for the Reddy third-order plate theory (1984a, b, 1987) for cross-ply rectangular plates. They used the state space approach in conjunction with the Lèvy method to solve the governing equations under various boundary conditions. Again, the temperature was assumed to vary linearly through the thickness.

All the aforementioned analyses refer to the small strain models. The von Kármán theory for large transverse deflection (of the order of the thickness of the plate) makes use of the non-linear strain displacement relations, in which the quadratic terms in the slopes of the deflection are retained while all other non-linear terms are neglected (see Reddy, 1997). Several analyses for laminated composite plates and for homogeneous isotropic plates have been reported. For a more detailed review, the reader is referred to the classical review by Tauchert (1991). To the authors' knowledge, there exist no results for the dynamic thermomechanical analysis of functionally graded plates, in the literature. Functionally graded plates are multiphase material plates, constructed so that the interface effects are mitigated by providing a continuous variation in the material properties through the thickness. The property variations are so designed as to meet some functional requirement, typically, a lowering of the thermal stress, the thermally induced deflections or vibration amplitudes.

Thermally induced vibration of a rectangular plate with one edge fixed and the other three edges simply supported was investigated by Jadeja and Loo (1974). Solutions for the case of surface heating were obtained using the Galerkin procedure. In the case of non-linear dynamic analysis, the von Kármán plate theory has been applied with the displacement field corresponding to the classical plate theory. Again, no results exist for the case of through-thickness material property varying plates using the von Kármán non-linearity in conjunction with the displacement field of the first order shear deformation plate theory. Most analyses corresponding to heterogeneous isotropic plates have been limited to plates with temperature sensitive material properties, and not spatially varying properties.

Finot and Suresh (1996) analyzed the response of multi-layered plates and fgm plates subjected to small and large deformation during temperature excursions. They examined general bilayer and trilayer plates with comparable layer thickness, with and without graded interfaces, all within the context of classical Kirchhoff theory for thin plates. They obtained closed-form solutions for stress–curvature relationships for the trilayer and graded isotropic elastic plates. They also analyzed plastic flow within these plates, as the temperature was varied.

Geometrically nonlinear transient analysis of isotropic and composite laminates have been reported in literature. To the authors' knowledge there are no previously reported results for the nonlinear, dynamic analysis of plates made of functionally graded materials, under thermal and mechanical loading. In this paper, we make use of the shear deformable element developed by Reddy (1984a) for the von Kármán plate theory. Numerical results are presented to show the parametric effect of material properties, plate thickness, nonlinearity, boundary conditions, mechanical loading, and temperature fields on the transient analysis of fgm plates. These results are important from the point of view of the design of thermal barrier materials. Analyzing the transient response of graded materials will help in designing

sensors and actuators to control vibrations. In the present paper, we examine the thermoelastostatic and thermoelastodynamic response of plates subjected to pressure loading and thickness varying temperature fields. The thickness variation of the temperature field comes about also due to the variation of the thermal properties.

2. EQUATIONS OF MOTION AND FINITE ELEMENT MODEL

The equations of motion used here are based on the combination of the first order plate theory and the von Kármán strains (see Reddy, 1997). This theory predicts the global behavior accurately. The theory assumes that the transverse normal stress is negligible when compared to the other stress components, and normals to the plate midsurface before deformation remain straight but not necessarily normal to the midsurface after deformation.

The domain of the plate is such that the x and y coordinates are taken in the midplane of the plate and the displacements are assumed to be linear through the thickness—the z coordinate. Thus, the plate is modeled using an equivalent single layer theory. The displacement components are assumed to be of the following form (see Reddy, 1994b, 1997)

$$\begin{aligned} u_1 &= u(x, y, t) + z\phi_x(x, y, t) \\ u_2 &= v(x, y, t) + z\phi_y(x, y, t) \\ u_3 &= w(x, y, t) \end{aligned} \tag{1}$$

where t denotes time, u_1, u_2 and u_3 are the total displacements and (u, v, w) are the midplane displacements in the x, y and z directions, respectively, and ϕ_x and ϕ_y are the rotations of the yz and xz planes due to bending. The von Kármán plate theory accounts for moderately large deflections and small strains. The strains according to this theory are (using standard vector notation)

$$\begin{aligned} \varepsilon_1 &= \frac{\partial u}{\partial x} + \frac{1}{2}\left(\frac{\partial w}{\partial x}\right)^2 + z\frac{\partial \phi_x}{\partial x} \equiv \varepsilon_1^0 + z\varepsilon_1^1 \\ \varepsilon_2 &= \frac{\partial v}{\partial y} + \frac{1}{2}\left(\frac{\partial w}{\partial y}\right)^2 + z\frac{\partial \phi_y}{\partial y} \equiv \varepsilon_2^0 + z\varepsilon_2^1 \\ \varepsilon_6 &= \frac{\partial u}{\partial y} + \frac{\partial v}{\partial x} + \frac{\partial w}{\partial x}\frac{\partial w}{\partial y} + z\left(\frac{\partial \phi_x}{\partial y} + \frac{\partial \phi_y}{\partial x}\right) \equiv \varepsilon_6^0 + z\varepsilon_6^1 \\ \varepsilon_4 &= \phi_y + \frac{\partial w}{\partial y} \\ \varepsilon_5 &= \phi_x + \frac{\partial w}{\partial x} \end{aligned} \tag{2}$$

wherein, the squares of the first partial derivatives of u, v, ϕ_x and ϕ_y are neglected. ε_i^0 are the in-plane strains and ε_i^1 are the curvatures due to bending. The strain ε_3 does not enter the constitutive equations, due to the plane stress assumption. The transverse shear strains ε_4 and ε_5 are constant through the thickness of the plate.

The governing equations of motion are derived from Hamilton's principle. In the absence of body moments, surface shearing forces, and thermal loading, the equations are given by

$$\begin{aligned} N_{xx,x} + N_{xy,y} &= I_0 u_{,tt} + I_1 \phi_{x,tt} \\ N_{xy,x} + N_{yy,y} &= I_0 v_{,tt} + I_1 \phi_{y,tt} \\ Q_{x,x} + Q_{y,y} &= I_0 w_{,tt} + q(x, y, t) + \bar{N}(w, N) \end{aligned}$$

$$M_{xx,x}+M_{xy,y}-Q_1 = I_2\phi_{x,tt}+I_1u_{,tt}$$
$$M_{xy,x}+M_{yy,y}-Q_2 = I_2\phi_{y,tt}+I_1v_{,tt} \tag{3}$$

where I_0, I_1 and I_2 are the normal, coupled normal rotary, and rotary inertia coefficients, respectively, and a comma followed by a variable denotes differentiation with respect to that variable. Also, "q" is the applied load on the plate top/bottom surface, and $N_{xx,yy,xy}$ and $M_{xx,yy,xy}$ are the force and moment resultants whose definitions are made precise later. $\bar{N}$ is a nonlinear force resultant that is dependent on the force resultants $N_{xx,yy,xy}$.

The fgm plate is considered to be a single layer plate of uniform thickness. The properties of the plate are assumed to vary through the thickness of the plate. The property variation is assumed to be in terms of a simple power law distribution given by

$$P(z) = (P_c - P_m)\left(\frac{2z+h}{2h}\right)^n + P_m \tag{4}$$

where P_c and P_m are the corresponding properties of the ceramic and metal, and n is the volume fraction exponent which takes values greater than or equal to zero. The value of n equal to 0 represents a fully ceramic plate. The above power law assumption reflects a simple rule of mixtures used to obtain the effective properties of the ceramic–metal plate. The rule of mixtures applies only to the thickness direction. The density of the plate varies according to the power law, and the power law exponent may be varied to obtain different distributions of the component materials through the thickness of the plate. With the power-law variation in properties, the various inertias may be calculated as follows:

$$(I_0, I_1, I_2) = \int_{-(h/2)}^{h/2}\left((\rho^c-\rho^m)\left(\frac{2z+h}{2h}\right)(1, z, z^2)+\rho^m(1, z, z^2)\right)\mathrm{d}z \tag{5}$$

where quantities with superscripts, "m" and "c" correspond to the metal and ceramic, respectively. The metal content in the plate increases as the value of n increases. The N, Ms and Qs are the axial force, moment and shear force resultants, respectively. These are calculated from the following integral expressions:

$$(N_{\alpha\beta}, M_{\alpha\beta}) = \int_{-(h/2)}^{h/2}(1, z)\sigma_{\alpha\beta}\,\mathrm{d}z$$
$$(Q_x, Q_y) = \int_{-(h/2)}^{h/2}(\sigma_{xz}, \sigma_{yz})\,\mathrm{d}z \tag{6}$$

where α, β stand for x, y and $\bar{N}(w, N_{\alpha\beta})$ is the contribution due to the nonlinear terms,

$$\bar{N}(w, N_{\alpha\beta}) = \frac{\partial w}{\partial x}\left(\frac{\partial N_{xx}}{\partial x}+\frac{\partial N_{xy}}{\partial y}\right)+\frac{\partial w}{\partial y}\left(\frac{\partial N_{xy}}{\partial x}+\frac{\partial N_{yy}}{\partial y}\right) \tag{7}$$

If one plane of elastic symmetry parallel to the plane of the plate exists, the constitutive equations of the plate can be written in the form (purely mechanical loading)

$$\begin{Bmatrix}\{N\}\\ \{M\}\end{Bmatrix} = \begin{bmatrix}[A] & [B]\\ [B] & [D]\end{bmatrix}\begin{Bmatrix}\{\varepsilon^0\}\\ \{\varepsilon^1\}\end{Bmatrix} \tag{8}$$

In the case of thermal loading, the equations contain the thermal force resultants, $N^T_{\alpha\beta}$, and the thermal moment resultants, $M^T_{\alpha\beta}$, and are defined elsewhere in the paper. The

form of the equations will be given here, with the details of the finite element implementation in the Appendix.

$$\begin{Bmatrix} \{N+N^T\} \\ \{M+M^T\} \end{Bmatrix} = \begin{bmatrix} [A] & [B] \\ [B] & [D] \end{bmatrix} \begin{Bmatrix} \{\varepsilon^0\} \\ \{\varepsilon_1\} \end{Bmatrix} \tag{9}$$

$$\begin{Bmatrix} Q_y \\ Q_x \end{Bmatrix} = \begin{bmatrix} \bar{A}_{44} & \bar{A}_{45} \\ \bar{A}_{45} & \bar{A}_{55} \end{bmatrix} \begin{Bmatrix} \varepsilon_4 \\ \varepsilon_5 \end{Bmatrix} \tag{10}$$

where $[A]$, $[B]$, $[D]$ $(i,j = 1,2,6)$, and $\bar{A}_{ij}$ $(i,j = 4,5)$ are the inplane, bending–stretching coupling, bending, and thickness-shear stiffnesses, respectively:

$$(A_{ij}, B_{ij}, D_{ij}) = \int_{-(h/2)}^{h/2} \left((Q_{ij}^c - Q_{ij}^m) \left(\frac{2z+h}{2h} \right)^n (1, z, z^2) + Q_{ij}^m (1, z, z^2) \right) \mathrm{d}z \tag{11}$$

$$\bar{A}_{ij} = \int_{(h/2)}^{h/2} k_i k_j Q_{ij} \, \mathrm{d}z \tag{12}$$

k_i are the shear correction coefficients and Q_{ij} are the material constants. For the plate in consideration, the bending–twisting coupling terms vanish and so the terms A_{16}, A_{26}, B_{16}, B_{26}, D_{16}, and D_{26} are identically zero. With the above stiffnesses vanishing, the non-linear force deflection relationships are

$$\begin{aligned}
N_{xx} &= A_{11}\left(\frac{\partial u}{\partial x} + \frac{1}{2}\left(\frac{\partial w}{\partial x}\right)^2\right) + A_{12}\left(\frac{\partial v}{\partial y} + \frac{1}{2}\left(\frac{\partial w}{\partial y}\right)^2\right) + B_{11}\frac{\partial \phi_x}{\partial x} + B_{12}\frac{\partial \phi_y}{\partial y} \\
N_{yy} &= A_{12}\left(\frac{\partial u}{\partial x} + \frac{1}{2}\left(\frac{\partial w}{\partial x}\right)^2\right) + A_{22}\left(\frac{\partial v}{\partial y} + \frac{1}{2}\left(\frac{\partial w}{\partial y}\right)^2\right) + B_{12}\frac{\partial \phi_x}{\partial x} + B_{22}\frac{\partial \phi_y}{\partial y} \\
N_{xy} &= A_{66}\left(\frac{\partial u}{\partial y} + \frac{\partial v}{\partial x} + \frac{\partial w}{\partial x}\frac{\partial w}{\partial y}\right) + B_{66}\left(\frac{\partial \phi_x}{\partial y} + \frac{\partial \phi_y}{\partial x}\right) \\
M_{xx} &= B_{11}\left(\frac{\partial u}{\partial x} + \frac{1}{2}\left(\frac{\partial w}{\partial x}\right)^2\right) + B_{12}\left(\frac{\partial v}{\partial y} + \frac{1}{2}\left(\frac{\partial w}{\partial y}\right)^2\right) + D_{11}\frac{\partial \phi_x}{\partial x} + D_{12}\frac{\partial \phi_y}{\partial y} \\
M_{yy} &= B_{12}\left(\frac{\partial u}{\partial x} + \frac{1}{2}\left(\frac{\partial w}{\partial x}\right)^2\right) + B_{22}\left(\frac{\partial v}{\partial y} + \frac{1}{2}\left(\frac{\partial w}{\partial y}\right)^2\right) + D_{12}\frac{\partial \phi_x}{\partial x} + D_{22}\frac{\partial \phi_y}{\partial y} \\
M_{xy} &= B_{66}\left(\frac{\partial u}{\partial y} + \frac{\partial v}{\partial x} + \frac{\partial w}{\partial x}\frac{\partial w}{\partial y}\right) + D_{66}\left(\frac{\partial \phi_x}{\partial y} + \frac{\partial \phi_y}{\partial x}\right) \\
Q_x &= A_{55}\left(\phi_x + \frac{\partial w}{\partial x}\right) \\
Q_y &= A_{44}\left(\phi_y + \frac{\partial w}{\partial y}\right)
\end{aligned} \tag{13}$$

The finite element model of the above equations may be derived by substituting the element approximations of the generalized displacements $(u, v, w, \phi_x \phi_y)$ into the appropriate weak forms of the five governing equations of motion. The element equations of motion are (see Reddy, 1992, 1997)

$$\sum_{\beta=1}^{5}\sum_{j=1}^{n(\beta)} K_{ij}^{\alpha\beta}\Delta_j^{\beta} + \sum_{\beta=1}^{5}\sum_{j=1}^{n(\beta)} M_{ij}^{\alpha\beta}\ddot{\Delta}_j^{\beta} = F_i^{\alpha} \tag{14}$$

The expressions for the individual finite element stiffness matrices are listed in the Appendix.

2.1. *Thermal analysis*

The thermal analysis is conducted by imposing constant surface temperatures at the ceramic and metal rich surfaces. The variation of temperature is assumed to occur in the thickness direction only. The temperature is assumed to be constant in the plane of the plate. The thermal analysis is carried out by first solving a simple steady state heat transfer equation through the thickness of the plate. In this problem, all the quantities are non-dimensionalized, such that the non-dimensional temperature variable varied between 0 and 1 across the non-dimensional domain of unit length. The problem is reduced to one with Dirichlet boundary conditions, with two independent parameters, namely the ratio of the thermal conductivity of the two materials, ρ_k, and the volume fraction index, n. The equation for the temperature through the thickness is as follows:

$$-\frac{\mathrm{d}}{\mathrm{d}z}\left(k(z)\frac{\mathrm{d}T}{\mathrm{d}z}\right) = 0 \tag{15}$$

where $T = T_c$ at $z = h/2$ and $T = T_m$ at $z = -h/2$.

In the present analysis, in addition to the uniform loading, the plate is subjected to a temperature field where the ceramic rich top surface is held at 300°C and the metal rich bottom surface is held at 20°C. A stress free temperature $T_0 = 0$°C is assumed. The materials are assumed to be perfectly elastic throughout the deformation. The temperature field imposed on the fgm plate gives rise to additional terms due to the von Kármán nonlinearity. To see this, consider the statement of virtual work in the absence of external mechanical loading. The material is assumed to be isotropic and therefore, the matrix representation of the thermal conductivity tensor is diagonal. In view of this, and the plane stress assumption, the temperature terms corresponding to ε_{11} and ε_{22} are the only remaining terms. To include the temperature terms, we define the thermal resultants, N_{xx}^T and M_{xx}^T. (Note that the thermal resultants corresponding to the y direction are the same as those of x, because of isotropy and also, the resultant corresponding to the xy term is zero.)

$$\int_{-(h/2)}^{h/2} \alpha C_{11}(1+\nu)(T-T_0)(1,z)\,\mathrm{d}z = (N^T, M^T) \tag{16}$$

With the above definitions, we have the following contribution to the thermal source terms of the standard finite element system of equations:

$$\int_V \sigma_{ij}^T \delta\varepsilon_{ij}\,\mathrm{d}V = \int_\Omega \left(N_{xx}^T\left[\frac{\partial\delta u}{\partial x} + \frac{\partial w}{\partial x}\frac{\partial\delta w}{\partial x}\right] + N_{yy}^T\left[\frac{\partial\delta v}{\partial y} + \frac{\partial w}{\partial y}\frac{\partial\delta w}{\partial y}\right]\right) + \left(M_{xx}^T\left[\frac{\partial\delta\psi_x}{\partial x}\right] + M_{yy}^T\left[\frac{\partial\delta\psi_y}{\partial y}\right]\right)\mathrm{d}A \tag{17}$$

$$\int_V \sigma_{ij}^T \delta\varepsilon_{ij}\,\mathrm{d}V = \int_\Omega \left(N^T\left[\frac{\partial\delta u}{\partial x} + \frac{\partial\delta v}{\partial y} + \frac{\partial w}{\partial x}\frac{\partial\delta w}{\partial x} + \frac{\partial w}{\partial y}\frac{\partial\delta w}{\partial y}\right] + M^T\left[\frac{\partial\delta\psi_x}{\partial x} + \frac{\partial\delta\psi_y}{\partial y}\right]\right)\mathrm{d}A \tag{18}$$

The temperature terms are included into the source terms of the element equations as follows:

$$\delta u: \int_{\Omega_e} (N^T)\frac{\partial \psi_i}{\partial x}\,\mathrm{d}x\,\mathrm{d}y$$

$$\delta v: \int_{\Omega_e} (N^T)\frac{\partial \psi_i}{\partial y}\,\mathrm{d}x\,\mathrm{d}y$$

$$\delta w: \sum_{j=1}^{n}\int_{\Omega_e} (N^T)\left(\frac{\partial \psi_i}{\partial x}\frac{\partial \psi_j}{\partial x}+\frac{\partial \psi_i}{\partial y}\frac{\partial \psi_j}{\partial y}\right)w_j\,\mathrm{d}x\,\mathrm{d}y$$

$$\delta \phi_x: \int_{\Omega_e} (M^T)\frac{\partial \psi_i}{\partial x}\,\mathrm{d}x\,\mathrm{d}y$$

$$\delta \phi_y: \int_{\Omega_e} (M^T)\frac{\partial \psi_i}{\partial y}\,\mathrm{d}x\,\mathrm{d}y \tag{19}$$

The thermal source term corresponding to the deflection is non-linear. This non-linearity is significant at high temperatures and coupled with the various thermal properties of the materials, can lead to response of the graded plates that is not intermediate to that of the metal and ceramic. There are two ways in which one can include the thermal source terms. In the first method, the nodal values w_j, i.e., the deflection, can be treated as unknowns and the resulting force term is transferred to the left hand side of the standard finite element basis functions. Thus the term is included into the direct stiffness matrix. This does not require a recomputation of the tangent stiffness matrix. Alternatively, the nodal values w_j can be retained on the right hand side and evaluated using those corresponding to the previous iteration. Thus, the thermal force term corresponding to the deflection is nonlinear. This in turn requires a recomputation of the tangent stiffness matrix corresponding to the third equilibrium equation. The two options discussed above were implemented in solving the thermoelastic problem for the fgm plate. At convergence, the difference between the results is found to be negligible, though, we may regard the first option as being more accurate and simpler to implement.

3. NUMERICAL RESULTS

3.1. *Static analysis*

In the present study, the four-noded rectangular isoparametric element was employed. The element has five degrees of freedom, three midplane displacements (u, v, w) and the two midplane rotations (ϕ_x, ϕ_y). Because the element accounts for the transverse shear strains, reduced integration is employed to evaluate the shear terms numerically. In the dynamic analysis, the static solution is used as the initial conditions and damping is neglected.

Figure 1 shows the geometry of the plate, the computational domain, and the boundary conditions used in the static problem. The static analysis was performed on a square plate

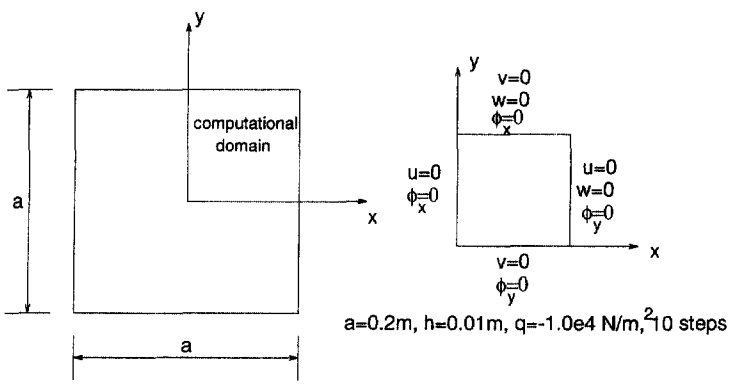

Fig. 1. A simply supported square plate with a quadrant as the computational domain.

of side ("a") 0.2 m and thickness ("h") 0.01 m. A regular mesh of 8×8 linear elements was chosen after convergence studies. The boundary conditions corresponding to the quarter plate model are shown in Fig. 1. The value of the uniformly distributed loading chosen was equal to 0.01×10^6 N/m^2. The results were plotted after ten loadsteps. The analysis is performed for different values of the volume fraction exponent. The results are presented in terms of non-dimensionalized stress and deflection. The various non-dimensionalized parameters used are

$$\text{center deflection (static) } \bar{w}: \quad \frac{w}{h}$$

$$\text{load parameter } P: \quad \frac{q_0 a^4}{E_m h^4}$$

$$\text{axial stress } \sigma_{xx}: \quad \frac{\sigma_{xx} h^2}{|q_0| a^2}$$

$$\text{thickness coordinate } \bar{z}: \quad \frac{z}{h}$$

where q is the applied mechanical load, a is the length of the plate, h is the plate thickness. The static analysis was conducted for two combinations of ceramic and metal. The first set of materials chosen were aluminum and zirconia. The second combination of materials consisted of aluminum and alumina. The Young's modulus, Poisson's ratio, density, conductivity and coefficient of thermal expansion, are for aluminum: 70 GPa, 0.3, 2707 kg/m^3, 204 W/mK, 23.0×10^{-6}/°C, alumina: 380 GPa, 0.3, 3800 kg/m^3, 10.4 W/mK, 7.4×10^{-6}/°C, for zirconia: 151 GPa, 0.3, 3000 kg/m^3, 2.09 W/mK, 10.0×10^{-6}/°C, respectively. Note that the Poisson's ratio was chosen to be 0.3 for simplicity. The thermal conductivity ratio for the two different ceramic–metal pairs chosen is significantly different. The conductivity ratios are 19.6 and 97.6, respectively. Thus, the temperature variation across the thickness of the plates is vastly different for the two cases, even though the same values of temperature were imposed on the top and bottom surfaces. The plate is assumed to be simply supported on all its edges, and the boundary conditions imposed on the edges are shown in Fig. 1. Note, that due to symmetry, only one quarter of the plate is used. There is no symmetry across the midplane, since the properties vary in a continuous manner through the thickness of the plate. In all cases, the lower surface of the plate is assumed to be metal rich and the top surface is assumed to be 100% ceramic. The ceramic surface is exposed to a temperature of 300°C and the lower metallic surface is exposed to a temperature of 20°C. A mechanical pressure loading q is also applied on the top surface of the plate.

Figure 2 shows the volume fraction of metallic phase, through the thickness. Note that the thickness coordinate has been non-dimensionalized. Figure 3 shows the variation of the temperature through the thickness of the aluminum–zirconia plates for various values of the volume fraction exponent, n. The temperature distribution was obtained by solving the one-dimensional heat conduction equation through the thickness, by assuming that the conductivity varies according to eqn (4). The conduction equation was solved by imposing the temperature boundary conditions at the top and bottom surface of the plate. It is assumed that at any value of the thickness coordinate, the temperature is the same at all points in the plane. It is seen that the temperature in the plates with both ceramic and metal is always greater than that corresponding to a fully ceramic or fully metallic plate. Further, the temperature at any location through the thickness of the alumina–zirconia plates was found to be less than that in the aluminum–alumina plates.

Figure 4 shows the variation of the non-dimensional center deflection with load for the aluminum–zirconia plates. Analysis was also performed for aluminum–alumina plates. We will present only the significant results or differences in the response of plates with the different material combinations. This difference is expected to be mainly due to the large thermal expansion ratios. The applied pressure load is increased in each load step, and the

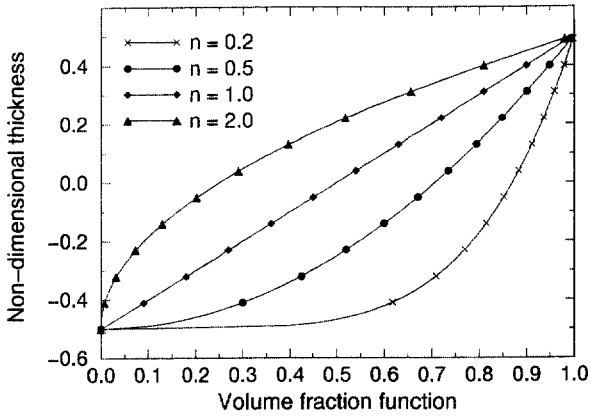

Fig. 2. Variation of the volume fraction function $((2z+h)/2h)^n$ through the non-dimensionalized thickness.

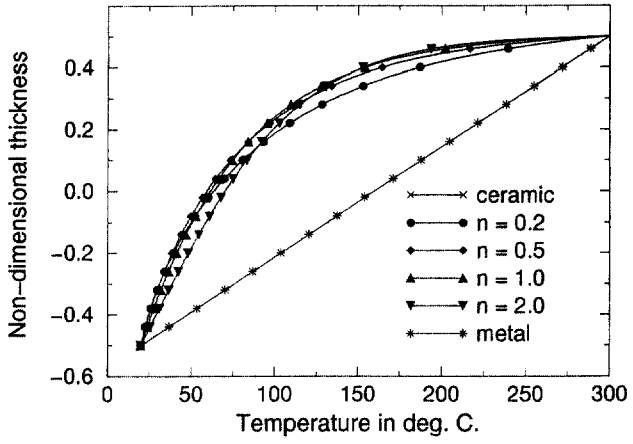

Fig. 3. Temperature field through the thickness of the fgm plate (aluminum–zirconia).

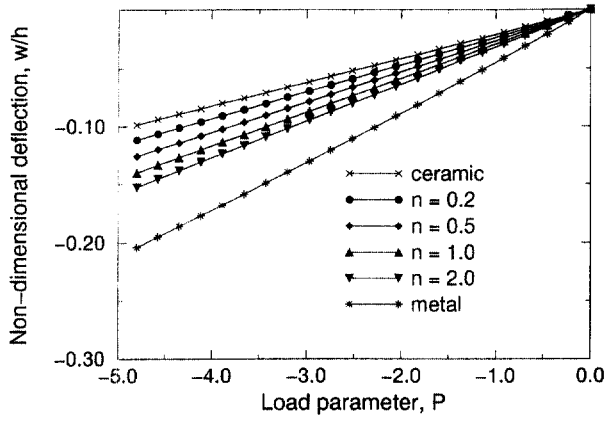

Fig. 4. Non-dimensionalized center deflection with load parameter for fgm plate, for various values of volume fraction exponent (aluminum–zirconia).

solution is obtained by an iterative procedure. At any load step, the assumed solution at the beginning of the nonlinear iteration is taken to be the converged solution at the previous load step. This reduces the number of iterations required and also increases the accuracy,

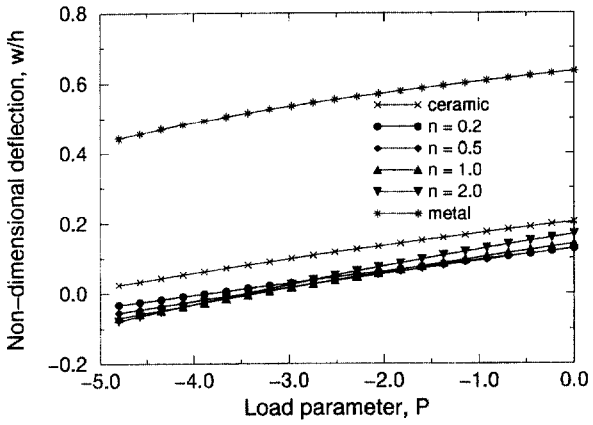

Fig. 5. Center deflection of simply supported fgm plate under uniform load and temperature field (aluminum–zirconia).

as compared to an arbitrary guess solution at each load step. In each case, the non-dimensionalization is carried out using the properties of the metal. In this case, the non-dimensional center deflection increases with pressure load. For the magnitude of the load chosen, the behavior was found to be linear. The effect of nonlinearity will be shown later. For both material pairs, the deflection of the metallic plate was found to be of the largest magnitude and that of the ceramic plate, of the smallest magnitude. All the plates with intermediate properties undergo corresponding intermediate values of center deflection. This is expected because the metallic plate is the one with the lowest stiffness and the ceramic plate is the one with the highest stiffness.

Figure 5 shows the variation of the center deflection with the mechanical load in the presence of the temperature field through the thickness of the aluminum–zirconia plate. Both the load and the center deflection are appropriately non-dimensionalized. It is important to observe that the through thickness temperature distribution for a fully ceramic plate coincides with that of a fully metal plate. This is because the plate for these two cases is fully homogeneous and the solution to the equations for temperature do not depend on the thermal conductivity. In both these cases, the distribution is linear. Now, excursions from this linear distribution are obtained by changing the volume fraction index. It is expected that the distribution will reach an extremum in terms of the average behavior, at some volume fraction index, and then turn back to the linear behavior. Thus, for a given pair of materials, there is a particular volume fraction that will extremize the deflection, under the same mechanical load. The non-dimensional deflection tends toward the negative side as the mechanical load increases. For the chosen temperature difference, the temperature effects on deflection reduce with increasing pressure loads. Note that the center deflection is reduced to zero for load parameter between -3 and -5 for the plates with different values of volume fraction exponent.

Note that the deflection of the plates under thermomechanical loading is positive. This is because, the thermal expansion at the top surface is higher due to the higher temperature, and this expansion results in an upward deflection of the plate. Note that the thermal strain in the ceramic rich portion may be comparable to that in the metal rich region (lower temperature) because the ceramic has a lower coefficient of thermal expansion than the metal. The deflection therefore depends on the product of the temperature and the thermal expansion coefficient. Therefore, the response of the graded plates is not intermediate to the metal and ceramic plates. The purely mechanical load is applied downwards (negative). Also, note that the center deflection of both the metallic and the ceramic plates is higher in magnitude than the graded plates. The deflection of the fgm plate corresponding to $n = 0.5$ seems to be a minimum. Note that the temperature profiles for the various plates are close to each other, and this probably is the reason why the deflections under temperature field for the various graded plates are also close to each other.

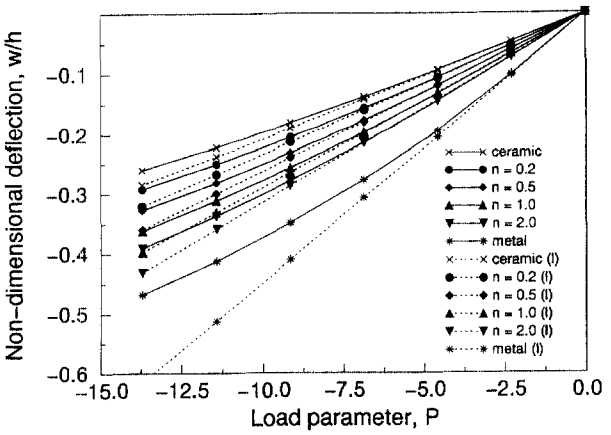

Fig. 6. Non-dimensional center deflection with load parameter for fgm plate under uniform loading—linear/nonlinear analysis (aluminum–zirconia).

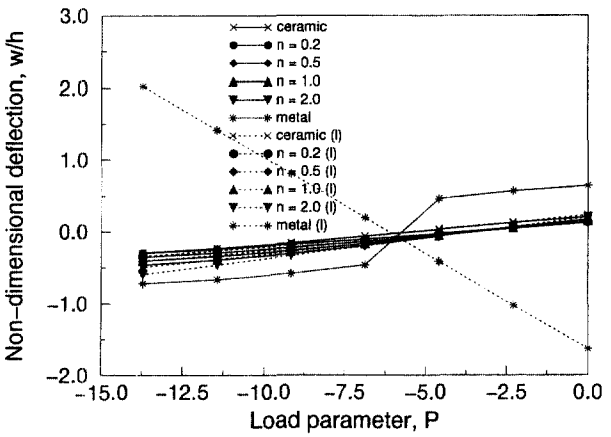

Fig. 7. Non-dimensional center deflection with load parameter for fgm plate under uniform loading and temperature field—linear/nonlinear analysis (aluminum–zirconia).

Figures 6 and 7 show the comparison between the linear and non-linear analysis, under mechanical loading and under thermal loading. The linear analysis always overpredicts the deflection magnitude in the pressure loading case, and the difference increases as the plate becomes more and more metallic. The analysis was carried out at a load of -10^5 N/m^2, with five load steps. Any applied load greater in magnitude than this load, will result in an increased deviation from the linear behavior. The effect of nonlinearity does not seem to be very much pronounced when the temperature field is applied. At zero mechanical load, the metallic plate undergoes upward deflection with the largest magnitude and this reduces as the pressure load is applied.

Figures 8 and 9 represent the behavior of the non-dimensional center deflection with changing plate side to thickness ratio. The analysis was carried out with a load of -1×10^6 N/m^2, with one loadstep. For all plates, the center deflection asymptotically reaches the same value for $(a/h) = 150$, when a purely mechanical loading is applied and this asymptotic behavior is reached for plates with $(a/h) = 75$, when the temperature field is also imposed.

Figures 10 and 11 contain the plots of the axial stress through the thickness of the plate under uniform loading applied on the top surface. Under the application of the pressure loading, the stresses are compressive at the top surface and tensile at the bottom surface. For the different volume fraction exponents chosen, the plate corresponding to $n = 2.0$ yielded the maximum compressive stress at the top surface. This is the ceramic rich surface. Note that ceramics are weaker in tension than in compression. The stress profiles

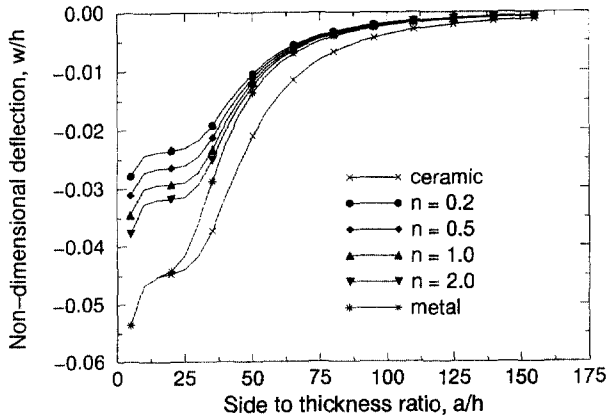

Fig. 8. Non-dimensional center deflection with side to thickness ratio for fgm plate under uniform loading (aluminum–zirconia).

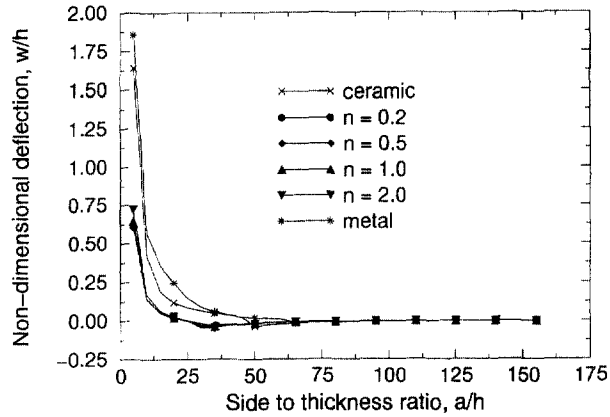

Fig. 9. Non-dimensional center deflection with side to thickness ratio for fgm plate under uniform loading and temperature field (aluminum–zirconia).

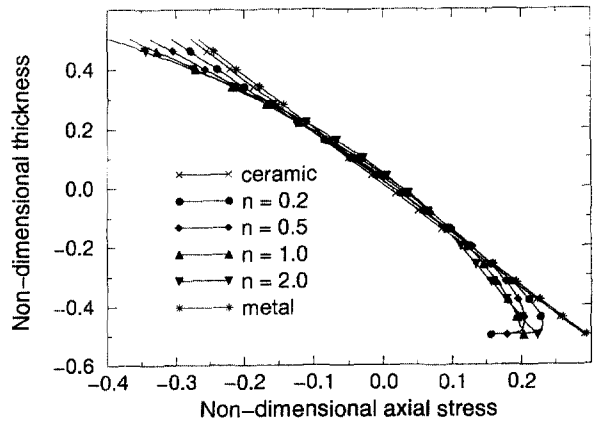

Fig. 10. Non-dimensional axial stresses in a simply supported square fgm plate under uniform loading of -1×10^4 N/m^2, 10 loadsteps (aluminum–zirconia).

under thermal loading are shown in Fig. 11. In this case, the nature of the profile changes drastically for the metallic plate, and the magnitude of the compressive stress increases for the fgm plates. Again, except for the ceramic plates, the stress profiles are close to each other, for the graded plates. Note that the stresses in the latter case are again compressive,

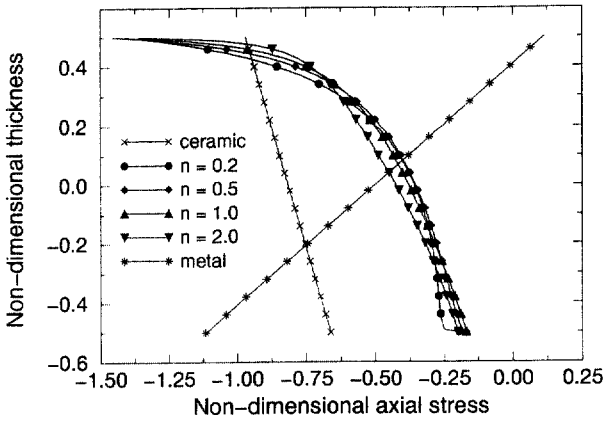

Fig. 11. Non-dimensional axial stresses in a simply supported square fgm plate under uniform loading of -1×10^4 N/m^2, 10 loadsteps and temperature field (aluminum–zirconia).

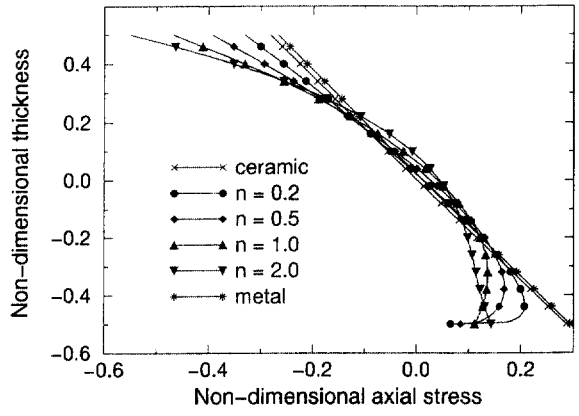

Fig. 12. Non-dimensional axial stresses in a simply supported square fgm plate under uniform loading of -1×10^4 N/m^2, 10 loadsteps (aluminum–alumina).

but with a higher magnitude, and this is because of the elastic strain which is the difference between the total strain and the thermal strain.

Figure 12 shows similar behavior to Fig. 10, except for the magnitudes. In both cases, the fgm plate corresponding to $n = 2.0$ experiences the maximum compressive stress at the top surface and the metallic and ceramic plates experience the maximum tensile stress at the bottom surface. For the case of aluminum–alumina (Fig. 13), the ratio of thermal conductivity is 19.6 and the temperatures are higher than in the case of aluminum–zirconia, and the compressive behavior in the whole domain is more pronounced as compared to Al–Z plates. The stress profiles are less clustered in Al–Z plates, even though the temperature profiles seem to be close to each other. The difference in stress patterns should be mainly due to the material properties. When no temperature field is applied, the plate with $n = 2.0$ experiences the maximum top surface compressive stress, but when the temperature field is also applied, the maximum is attained by the plate corresponding to $n = 0.2$. Figure 14 shows the non-dimensional axial stress in aluminum–alumina plate at higher value of the applied load (-10×10^4 N/m^2, 20th loadstep) under imposed temperature field. In the case where only the mechanical load was applied, the non-dimensional stress was almost the same as the one corresponding to Fig. 12.

3.2. *Dynamic response*

3.2.1. *Simply supported boundary conditions* Next, numerical experiments were performed to characterize the dynamic response of the fgm plate to suddenly applied uniform

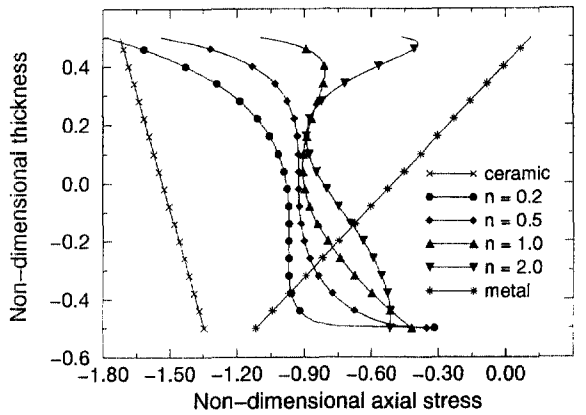

Fig. 13. Non-dimensional axial stresses in a simply supported square fgm plate under uniform loading of -1×10^4 N/m^2, 10 loadsteps and temperature field (aluminum–alumina).

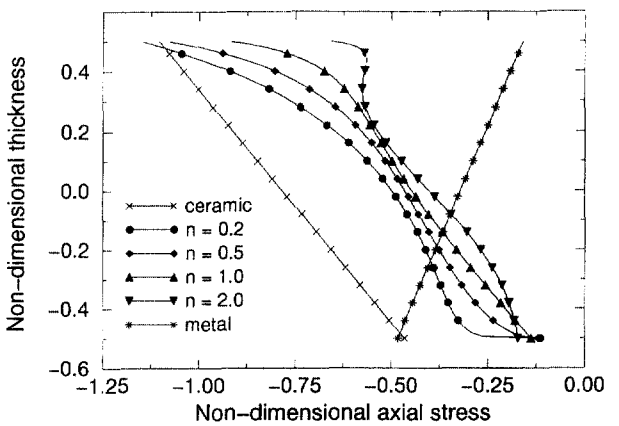

Fig. 14. Non-dimensional axial stresses in a simply supported square fgm plate under uniform loading of -10×10^4 N/m^2, 20 loadsteps and temperature field (aluminum–alumina).

pressure loading and also the case of suddenly applied load under an imposed temperature field. As mentioned earlier, the time derivatives in the semi-discrete model were approximated by using the Newmark direct integration method.

Since no estimate on the time step for the nonlinear analysis is available, the critical time step of a conditionally stable finite difference scheme was used as the starting time step, and a convergence study was conducted to select a time step that yielded a stable and accurate solution while keeping the computational time to a minimum. The estimate used in the present study is

$$\Delta t_1 \leqslant 0.25(\rho h/D)^{1/2}(\Delta x)^2 \tag{20}$$

Here $D = [(Eh^3)/12(1-\nu^2)]$, and Δx is the minimum distance between the element node points. This estimate is due to Leech (1965), and was derived for thin plates. The values of E and ρ used in the above estimates correspond to the smallest time step that could be obtained.

First, in order to prove the validity of the present formulation and the code developed, the results were obtained for isotropic plates and compared with those existing in literature. For this, the problem solved in the papers by Akay (1980) (using a mixed finite element) and Reddy (1983) (using the present formulation) was solved. The geometry of the plate and the various dimensions, boundary conditions are the same as in Fig. 1 for the case of the simply supported plates. For validating the code, a side length of 2.438 m, thickness

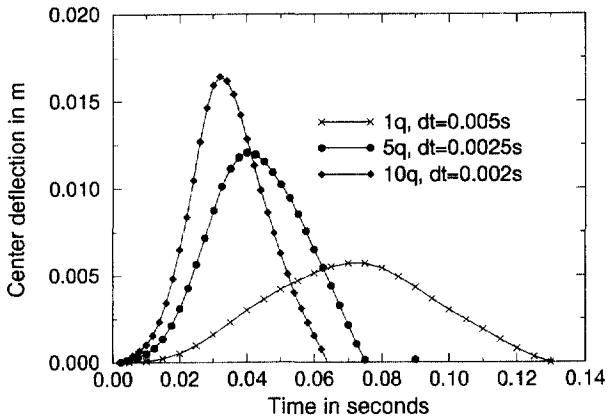

Fig. 15. Vibrations of simply supported isotropic plate under suddenly applied uniform loading—results of analysis by Akay and Reddy.

0.00635 m and a load of 4.882×10^6 N/m^2 were taken. The time steps used in the computations are indicated in the figure. For the analysis of the FGM plates, a side length of 0.2 m, thickness of 0.01 m and a load of -10^6 N/m^2 were considered. For all the cases, a timestep of 0.00001 s was used. The first set of values were used to verify the analysis due to Akay and Reddy. The second set of values were used to obtain the results presented in this paper.

A 2×2 uniform mesh of quadratic elements is used in the quarter plate with five degrees of freedom per node. The same mesh was used in the analyses by Akay and Reddy. The figure shows the geometry of the plate, along with the boundary conditions and the material properties used in the analysis. The load was applied after the first time step and held constant thereafter. After convergence studies, with linear and quadratic elements, a mesh of 8×8 bilinear elements was chosen for the results presented herein.

Figure 15 shows the response of the isotropic plate under suddenly applied uniform pressure loading. The results were generated during the present study in order to validate the code developed. Results of the present nonlinear analysis agree closely with the finite element results of Akay and those of Reddy. The plots of center deflection vs time for various loads are shown. The center deflection and time were non-dimensionalized according to the following expressions:

$$\text{center deflection } \bar{W}: \quad \frac{wE_m h}{q_0 a^2}$$

$$\text{time } \bar{t}: \quad \sqrt{\frac{E_m}{a^2 \rho_m}}$$

Figures 16 and 17 show the transient response of the aluminum–alumina plates, and Figs 18 and 19 show the dynamic response of the aluminum–zirconia plates. The higher the bending rigidity, the lower the magnitude of deflection. The amplitude of vibration is the maximum for the metallic plate and a minimum for the ceramic plate. It is seen that the amplitude of vibration increases smoothly as the amount of metal in the plate increases. Also, it is clear that the frequency of vibration of the ceramic plates is much higher than that of the metallic plates. When the sudden load is applied under a temperature field through the thickness the deflection changes, from negative to positive. Since the analysis is nonlinear, we cannot define a single natural frequency. The frequency of vibration of the surface heated plates appears to be a superposition of multiple frequencies. In order to obtain the response of the fgm plates under an imposed temperature field, the initial conditions are obtained from static analysis. The temperature field causes an upward deflection of the plates, and the load causes a downward deflection. Thus, vibrations occur

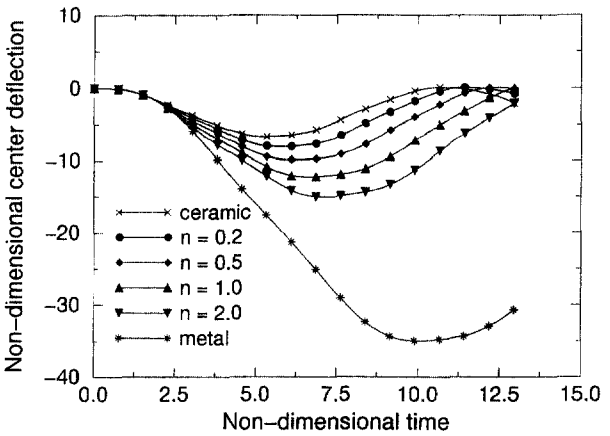

Fig. 16. Temporal evolution of center deflection of simply supported fgm plate under suddenly applied uniform loading of -1.0×10^6 N/m^2 (aluminum–alumina).

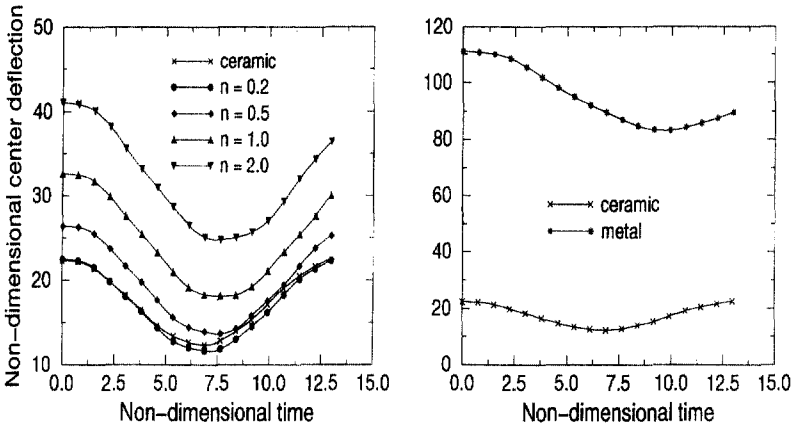

Fig. 17. Temporal evolution of center deflection of simply supported fgm plate under suddenly applied uniform loading of -1.0×10^6 N/m^2 and temperature field (aluminum–alumina).

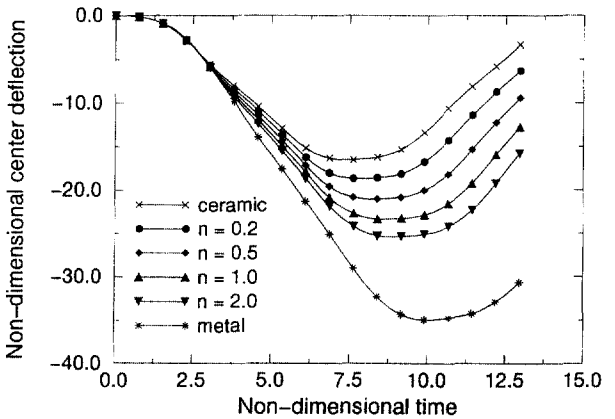

Fig. 18. Temporal evolution of center deflection of simply supported fgm plate under suddenly applied uniform loading of -1.0×10^6 N/m^2 (aluminum–zirconia).

about an equilibrium position which is displaced in the positive direction. One of the main inferences from the analysis is that the response of fgm plates is not intermediate to that of the metal and ceramic plates. This is due to the difference in bending stiffnesses and the thermal strains experienced by the various plates. Also, note that the coefficient of thermal

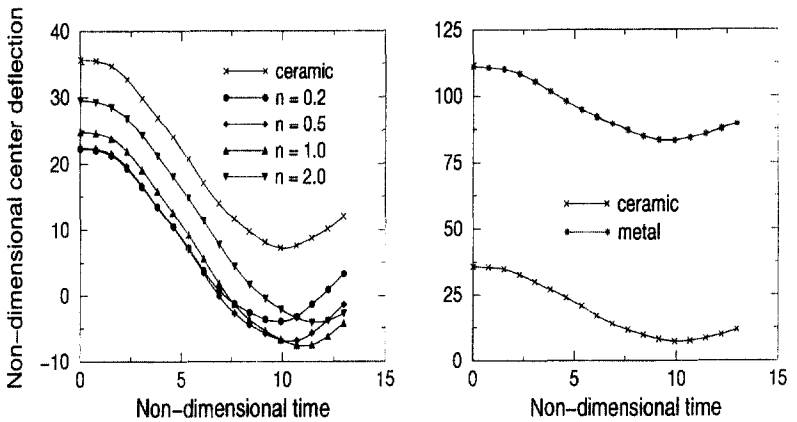

Fig. 19. Temporal evolution of center deflection of simply supported fgm plate under suddenly applied uniform loading of -1.0×10^6 N/m^2 and temperature field (aluminum–zirconia).

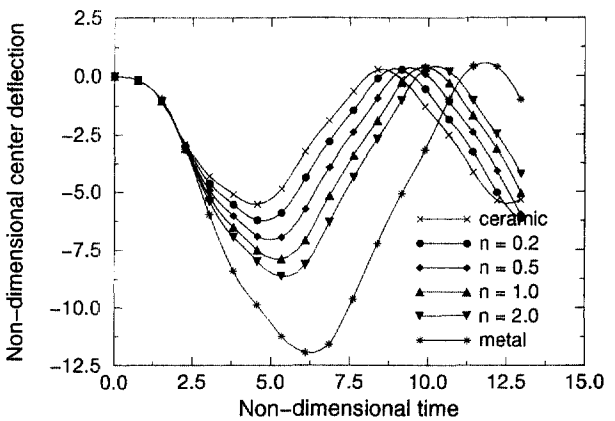

Fig. 20. Temporal evolution of center deflection of clamped fgm plate under suddenly applied uniform loading of -1.0×10^6 N/m^2 (aluminum–zirconia).

expansion increases as the metallic content increases, but the temperature for the graded plates is higher than that of the ceramic or the metal plate.

3.2.2. *Clamped boundary conditions* The computational domain for the dynamic analysis with clamped boundary conditions is the same as that of Fig. 1, except for some additional boundary conditions. The additional boundary conditions are as follows: on the top boundary, $u = 0$, $\phi_x = 0$ and, on the right edge, $v = 0$, $\phi_x = 0$. The analysis was performed for the same two material combinations. Since the effective stiffness of the clamped plates is higher than the simply supported plates, it is clearly seen that the deflections are much lower corresponding to the simply supported case. Also, the frequency of vibration is higher as compared to the simply supported plates. A timestep of 0.00001 s was used in the computations. Figures 20 and 21 show the temporal response of the plates under suddenly applied mechanical loading of -1.0×10^6 N/m^2.

4. CONCLUSIONS

The static and dynamic thermoelastic response of functionally graded material plates is studied. Nonlinearity has been restricted to the von Kármán type. The stress and deflection response of the plates have been analyzed under mechanical loading and thermal loading. The gradation of properties through the thickness is assumed to be of the power law type and comparisons have been made with homogeneous isotropic plates. Non-dimensional

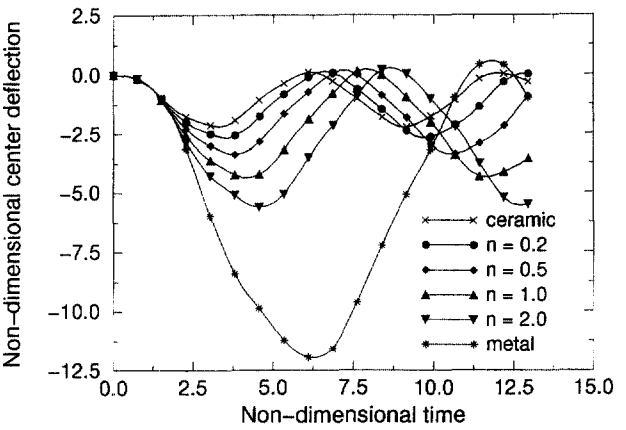

Fig. 21. Temporal evolution of center deflection of clamped fgm plate under suddenly applied uniform loading of -1.0×10^6 N/m^2 (aluminum–alumina).

stresses and deflection are computed for plates with two different ceramic–metal mixtures. It is seen that the basic response of the plates that correspond to properties intermediate to that of the metal and the ceramic, does not necessarily lie in between that of the ceramic and metal. The non-dimensional deflection was found to reach a minimum at a volume fraction index that depends on the properties and the ratio of the properties of the constituents. In the absence of thermal loading, the dynamic response of the graded plates is intermediate to that of the metal and ceramic plates. This is not the case when both thermal and mechanical loads are applied. This behavior is found to be true irrespective of boundary conditions. Thus, the gradients in material properties play an important role in determining the response of the fgm plates.

Acknowledgement—The authors wish to acknowledge the support for this research provided by AFOSR under Grant No. F49620-95-1-0342 with Texas A&M University.

REFERENCES

Akay, H. U. (1980) Dynamic large deflection analysis of plates using mixed finite elements. *Computers and Structures* **11**, 1–11.

Bapu Rao, M. N. (1979) Thermal bending of thick rectangular plates. *Nuclear Engineering Design* **54**, 115–118.

Boley, B. A. and Weiner, J. H. (1960) *Theory of Thermal Stresses*. Wiley, New York.

Das, Y. C. and Navaratna, D. R. (1962) Thermal bending of rectangular plate. *Journal of Aerospace Sciences* **29**, 1397–1399.

Das, Y. C. and Rath, B. K. (1972) Thermal bending of moderately thick rectangular plates. *AIAA Journal* **10**, 1349–1351.

De Leon, S. and Paris, F. (1987) Analysis of thermal stresses in plates with boundary element method. *Engineering Analysis* **4**, 199–203.

Finot, M. and Suresh, S. (1996) Small and large deformation of thick and thin-film multilayers: effects of layer geometry, plasticity and compositional gradients. *Journal of Mechanics and Physics of Solids* **44**(5), 683–721.

Jadeja, N. D. and Loo, T. C. (1974) Heat induced vibration of a rectangular plate. *Journal of Engineering Industry* **96**, 1015–1021.

Khdeir, A. A. and Reddy, J. N. (1991) Thermal stresses and deflections of cross-ply laminated plates using refined plate theories. *Journal of Thermal Stresses* **14**(4), 419–438.

Khdier, A. A., Ragab, M. D. and Reddy, J. N. (1992) Thermal effects on the response of cross-ply laminated shallow shells. *International Journal of Solids and Structures* **29**(5), 653–667.

Reddy, J. N. (1984a) Geometrically nonlinear transient analysis of laminated composite plates. *AIAA Journal* **21**(4), 621–629.

Reddy, J. N. (1984b) *Energy and Variational Methods in Applied Mechanics*. Wiley Interscience, New York.

Reddy, J. N. (1992) *Introduction to the Finite Element Method*. 2nd edn. McGraw-Hill, New York.

Reddy, J. N. (1997) *Mechanics of Laminated Composite Plates: Theory and Analysis*. CRC Press, Boca Raton, FL.

Reddy, J. N. and Chao, W. C. (1981) A comparison of closed-form and finite element solutions of thick, laminated, anisotropic rectangular plates. *Nuclear Engineering and Design* **64**, 153–167.

Reddy, J. N. and Hsu, Y. S. (1980) Effects of shear deformation and anisotropy on the thermal bending of layered composite plates. *Journal of Thermal Stresses* **3**, 475–493.

Reddy, J. N., Bert, C. W. and Hsu, Y. S. (1981) Thermoelasticity of circular cylindrical shells laminated of bimodulus composite materials. *Journal of Thermal Stresses* **4**, 155–177.

Schneider, P. J. (1955) Variation of maximum thermal stress in free plates. *Journal of Aeronautical Sciences* **22**, 872–873.
Tang, S. (1968) Thermal stresses in temperature dependent isotropic plates. *J. Spacecraft* **5**, 987–990.
Tauchert, T. R. (1986) Thermal stresses in plates—statistical problems. *Thermal Stresses*, ed. R. B. Hetnarski, Vol. I, pp. 23–137. North Holland, New York.
Tauchert, T. R. (1987) Thermal stresses in plates—dynamical problems. *Thermal Stresses*, ed. R. B. Hetnarski, Vol. II, pp. 23–137. North Holland, New York.
Tauchert, T. R. (1991) Thermally induced flexure, buckling and vibration of plates. *Applied Mechanics Reviews* **44**(8), 347–360.
Tsui, T. Y. and Ping Tong (1971) Stability of transient solution of moderately thick plate by finite difference method. *AIAA Journal* **9**, 2062–2063.

APPENDIX: FINITE ELEMENT MATRICES

The individual matrices appearing in the finite element model are as follows:

$$K_{ij}^{1\alpha} = \int_{\Omega^e} \left(\frac{\partial \psi_i}{\partial x} N_{1j}^{\alpha} + \frac{\partial \psi_i}{\partial y} N_{6j}^{\alpha} \right) \mathrm{d}x\,\mathrm{d}y$$

$$K_{ij}^{2\alpha} = \int_{\Omega^e} \left(\frac{\partial \psi_i}{\partial x} N_{6j}^{\alpha} + \frac{\partial \psi_i}{\partial y} N_{2j}^{\alpha} \right) \mathrm{d}x\,\mathrm{d}y$$

$$K_{ij}^{3\alpha} = \int_{\Omega^e} \left[\frac{\partial \psi_i}{\partial x} Q_{1j}^{\alpha} - \frac{\partial \psi_i}{\partial y} Q_{2j}^{\alpha} + \frac{\partial \psi_i}{\partial x} \left(N_{1j}^{\alpha} \frac{\partial w}{\partial x} + N_{6j}^{\alpha} \frac{\partial w}{\partial y} \right) + \frac{\partial \psi_i}{\partial y} \left(N_{6j}^{\alpha} \frac{\partial w}{\partial x} + N_{2j}^{\alpha} \frac{\partial w}{\partial y} \right) \right] \mathrm{d}x\,\mathrm{d}y$$

$$K_{ij}^{4\alpha} = \int_{\Omega^e} \left(\frac{\partial \psi_i}{\partial x} M_{1j}^{\alpha} + \frac{\partial \psi_i}{\partial y} M_{6j}^{\alpha} \right) \mathrm{d}x\,\mathrm{d}y + \int_{\Omega^e} Q_{1j}^{\alpha} \psi_i \,\mathrm{d}x\,\mathrm{d}y$$

$$K_{ij}^{5\alpha} = \int_{\Omega^e} \left(\frac{\partial \psi_i}{\partial x} M_{6j}^{\alpha} + \frac{\partial \psi_i}{\partial y} M_{2j}^{\alpha} \right) \mathrm{d}x\,\mathrm{d}y + \int_{\Omega^e} Q_{2j}^{\alpha} \psi_i \,\mathrm{d}x\,\mathrm{d}y \tag{21}$$

where, we have

$$N_{1j}^1 = A_{11} \frac{\partial \psi_j}{\partial x} \quad N_{1j}^2 = A_{12} \frac{\partial \psi_j}{\partial y} \quad N_{1j}^3 = \frac{A_{11}}{2} \frac{\partial w}{\partial x} \frac{\partial \psi_j}{\partial x} + \frac{A_{12}}{2} \frac{\partial w}{\partial y} \frac{\partial \psi_j}{\partial y}$$

$$N_{2j}^1 = A_{12} \frac{\partial \psi_j}{\partial x} \quad N_{2j}^2 = A_{22} \frac{\partial \psi_j}{\partial y} \quad N_{2j}^3 = \frac{A_{12}}{2} \frac{\partial w}{\partial x} \frac{\partial \psi_j}{\partial x} + \frac{A_{22}}{2} \frac{\partial w}{\partial y} \frac{\partial \psi_j}{\partial y}$$

$$N_{6j}^1 = A_{66} \frac{\partial \psi_j}{\partial x} \quad N_{6j}^2 = A_{66} \frac{\partial \psi_j}{\partial y} \quad N_{6j}^3 = \frac{A_{66}}{2} \frac{\partial w}{\partial x} \frac{\partial \psi_j}{\partial y} + \frac{A_{66}}{2} \frac{\partial w}{\partial y} \frac{\partial \psi_j}{\partial x}$$

$$M_{1j}^1 = B_{11} \frac{\partial \psi_j}{\partial x} \quad M_{1j}^2 = B_{12} \frac{\partial \psi_j}{\partial y} \quad M_{1j}^3 = \frac{B_{11}}{2} \frac{\partial w}{\partial x} \frac{\partial \psi_j}{\partial x} + \frac{B_{12}}{2} \frac{\partial w}{\partial y} \frac{\partial \psi_j}{\partial y}$$

$$M_{2j}^1 = B_{12} \frac{\partial \psi_j}{\partial x} \quad M_{2j}^2 = B_{22} \frac{\partial \psi_j}{\partial y} \quad M_{2j}^3 = \frac{B_{12}}{2} \frac{\partial w}{\partial x} \frac{\partial \psi_j}{\partial x} + \frac{B_{22}}{2} \frac{\partial w}{\partial y} \frac{\partial \psi_j}{\partial y}$$

$$M_{6j}^1 = B_{66} \frac{\partial \psi_j}{\partial y} \quad M_{6j}^2 = B_{66} \frac{\partial \psi_j}{\partial x} \quad M_{6j}^3 = \frac{B_{66}}{2} \frac{\partial w}{\partial x} \frac{\partial \psi_j}{\partial x} + \frac{B_{66}}{2} \frac{\partial w}{\partial y} \frac{\partial \psi_j}{\partial x}$$

$$Q_{1j}^1 = 0 \quad Q_{1j}^2 = 0 \quad Q_{1j}^3 = A_{55} \frac{\partial \psi_j}{\partial x}$$

$$Q_{2j}^1 = 0 \quad Q_{2j}^2 = 0 \quad Q_{2j}^3 = A_{44} \frac{\partial \psi_j}{\partial y} \tag{22}$$

$$N_{1j}^4 = B_{11} \frac{\partial \psi_j}{\partial x} \quad N_{1j}^5 = B_{12} \frac{\partial \psi_j}{\partial y} \quad N_{2j}^4 = B_{12} \frac{\partial \psi_j}{\partial x} \quad N_{2j}^5 = B_{22} \frac{\partial \psi_j}{\partial y}$$

$$N_{6j}^4 = B_{66} \frac{\partial \psi_j}{\partial y} \quad N_{6j}^5 = B_{66} \frac{\partial \psi_j}{\partial x} \quad M_{1j}^4 = D_{11} \frac{\partial \psi_j}{\partial x} \quad M_{1j}^5 = D_{12} \frac{\partial \psi_j}{\partial y}$$

$$M_{2j}^4 = D_{12} \frac{\partial \psi_j}{\partial x} \quad M_{2j}^5 = D_{22} \frac{\partial \psi_j}{\partial y} \quad M_{6j}^4 = D_{66} \frac{\partial \psi_j}{\partial y} \quad M_{6j}^5 = D_{66} \frac{\partial \psi_j}{\partial x}$$

$$Q_{1j}^4 = A_{55} \psi_j \quad Q_{1j}^5 = 0 \quad Q_{2j}^5 = A_{44} \psi_j \quad Q_{2j}^4 = 0 \tag{23}$$

In the expressions above, ψ_i and ψ_j are the finite element interpolation functions in the expansion

$$(u, v, w, \phi_x, \phi_y) = \sum_{j=1}^{n} (u_j(t), v_j(t), w_j(t), \phi_{xj}(t), \phi_{yj}(t))\psi_j(x, y) \tag{24}$$

Note that for the sake of simplicity, the same interpolation function has been used for each of the generalized midplane displacements. The finite element equations are nonlinear. To complete the discretization, the time derivatives appearing in the semidiscrete form are approximated by the use of the Newmark direct integration method, with $\alpha = 0.5$ and $\beta = 0.25$ (corresponding to the constant average acceleration method). The scheme, although unconditionally stable for linear problems, is not proven stable for all nonlinear problems. The nonlinear element equations are then solved using the Newton–Raphson method. This involves the derivation of the tangent stiffness matrix. For the sake of brevity, the elements of the tangent stiffness matrix have been omitted.

The expressions for the plate stiffnesses are given below:

$$A_{ij} = (Q_{ij}^{c} - Q_{ij}^{m}) \left(\frac{h}{n+1} \right) + Q_{ij}^{m} h$$

$$B_{ij} = (Q_{ij}^{c} - Q_{ij}^{m}) \left(\frac{nh^2}{2(n-1)(n+2)} \right)$$

$$D_{ij} = (Q_{ij}^{c} - Q_{ij}^{m}) \left(\frac{(2+n+n^2)h^2}{4(n+1)(n+2)(n+3)} \right) + Q_{ij}^{m} \frac{h^3}{24}$$

The expression for the various inertias I_0, I_1, I_2, may be obtained by replacing the Qs in the above equations by the corresponding densities.